Scientific Journal of Riga Technical University
Power and Electrical Engineering
2011
Volume 29

Lossless Dynamic Models of the Quasi-Z-Source Converter Family

Dmitri Vinnikov, *Tallinn University of Technology*, Oleksandr Husev, *Chernihiv State Technological University*, Indrek Roasto, *Tallinn University of Technology*

***Abstract* – This paper is devoted to the quasi-Z-source (qZS) converter family. Recently, the qZS-converters have attracted attention because of their specific properties of voltage boost and buck functions with a single switching stage, which could be especially beneficial in renewable energy applications. As main representatives of the qZS-converter family, the traditional quasi-Z-source inverter as well as two novel extended boost quasi-Z-source inverters are discussed. Lossless dynamic models of these topologies are presented and analyzed.**

***Keywords* – quasi-Z-source inverter (qZSI), capacitor assisted extended boost qZSI, diode assisted extended boost qZSI.**

I. INTRODUCTION

Recently, the quasi-Z-source inverter (qZSI) topology (Fig. 1*a*) has attracted attention because of its specific properties of voltage boost and buck functions with a single switching stage [1-4]. The qZSI also features such advantages as continuous input current, low or no inrush current during start-up, high immunity against EMI noise and misgating. As a result, the qZSI has become a very attractive choice for renewable and alternative energy applications, where the reliability and reduced number of energy conversion stages could play a vital role.

The conception of extending the qZSI boost capability without increasing the number of active switches has been recently proposed by several authors [5-12]. These new converters are known as cascaded (or extended boost) qZSIs and are generally classified as capacitor assisted and diode assisted. The topology of a capacitor assisted extended boost qZSI (CAEB qZSI, Fig. 1*b*) was derived by the adding of one diode (D_2), one inductor (L_3) and two capacitors (C_3 and C_4) to the traditional qZSI. The topology of a diode assisted extended boost qZSI (DAEB qZSI shown in Fig. 1*c*) was derived by the adding of one capacitor (C_3), one inductor (L_3) and two diodes (D_2 and D_3) to the traditional qZSI.

These three topologies (Fig. 1) have a common property - the input inductor L_1 that buffers the source current. It means that during the continuous conduction mode (CCM) the input current of the converter never drops to zero, thus featuring the reduced stress of the input voltage source.

Since each of these three topologies has a different number of passive components in the qZS-networks, a detailed analysis of component losses and their impact on a converter's operating properties is especially topical to obtain higher energy efficiencies. In [12] it was stated that for the same operating parameters and component values the twofold boost of the input voltage could be realized at the efficiency of 93.9 %, 89.2 % and 89.3 % for the traditional, CAEB and DAEB qZS-converters, respectively.

This paper is devoted to further investigation of the properties of the qZS-converter family and will provide a mathematical representation of the lossless dynamic models in order to study the transient stability of the presented topologies.

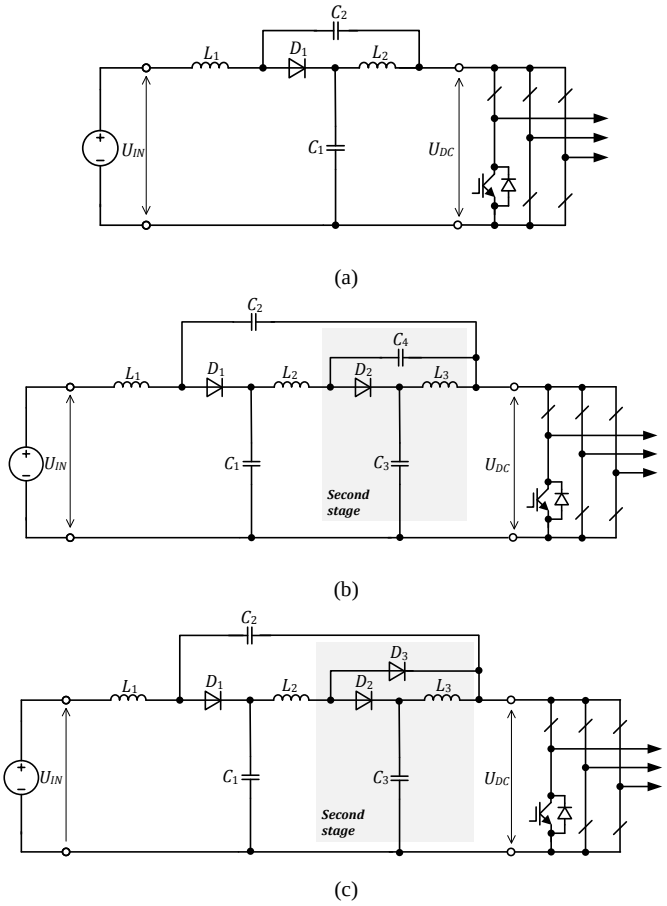

Fig. 1. Representatives of the qZS-converter family: traditional qZSI (a), capacitor assisted extended boost qZSI (b) and diode assisted extended boost qZSI (c).

II. TRADITIONAL QZS-CONVERTER

Fig. 2 illustrates a lossless dynamic model of the traditional qZS-converter, which regards the CCM, and in which the diode *D* (Fig. 1*a*) was replaced with the switch $\overline{S}$ and the full–bridge inverter by the switch *S*. Both switches work in synchronized manner.

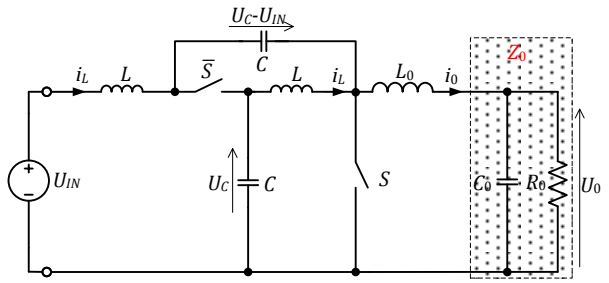

Fig. 2. Lossless dynamic model of the qZS-converter.

This model is described by the following differential equations:

- in the shoot-through state (intervals of length $D_0 \cdot T$):

$$\begin{bmatrix} L\frac{di_L}{dt} \\ C\frac{du_c}{dt} \\ L_0\frac{di_0}{dt} \end{bmatrix} = \underbrace{\begin{bmatrix} 0 & 1 & 0 \\ -1 & 0 & 0 \\ 0 & 0 & -Z_0 \end{bmatrix}}_{A_1} \cdot \underbrace{\begin{bmatrix} i_L \\ u_c \\ i_0 \end{bmatrix}}_{X} + \underbrace{\begin{bmatrix} 0 \\ 0 \\ 0 \end{bmatrix}}_{B_1} \cdot U\,, \qquad (1)$$

- in the active state (intervals of length $D_1 \cdot T$):

$$\begin{bmatrix} L\frac{di_L}{dt} \\ C\frac{du_c}{dt} \\ L_0\frac{di_0}{dt} \end{bmatrix} = \underbrace{\begin{bmatrix} 0 & -1 & 0 \\ 1 & 0 & -1 \\ 0 & 2 & -Z_0 \end{bmatrix}}_{A_2} \cdot \underbrace{\begin{bmatrix} i_L \\ u_c \\ i_0 \end{bmatrix}}_{X} + \underbrace{\begin{bmatrix} 1 \\ 0 \\ -1 \end{bmatrix}}_{B_2} \cdot U\,, \qquad (2)$$

where $U=U_{IN}$, and also $D_0+D_1=1$ (since the CCM is under consideration). A small signal model of the converter in the state space can be represented as [4]:

$$K\frac{d}{dt}X = A_1 X + B_1 U\,, \qquad (3)$$

in the shoot-through interval when $S=1$.

$$K\frac{d}{dt}X = A_2 X + B_2 U\,, \qquad (4)$$

in the active state interval when $S=0$.

Eqs. (3) and (4) can be recorded for small gains:

$$K\frac{d}{dt}\tilde{X} = A\tilde{x} + B\tilde{u} + \left[\left(A_1 - A_2\right)X + \left(B_1 - B_2\right)U\right]\cdot\tilde{d}\,, \qquad (5)$$

where: $B = B_1 \cdot D_0 + B_2 \cdot D_1$; $A = A_1 \cdot D_0 + A_2 \cdot D_1$.

Hence, taking into consideration matrixes A_1, A_2, B_1, B_2 included in Eq. (5) as well as the fact that in the case of the CCM $D_1=1-D_0$, we obtain:

$$\begin{bmatrix} L\frac{d\tilde{i}_L}{dt} \\ C\frac{d\tilde{u}_c}{dt} \\ L_0\frac{d\tilde{i}_0}{dt} \end{bmatrix} = \begin{bmatrix} 0 & 2D-1 & 0 \\ 1-2D & 0 & D-1 \\ 0 & 2-2D & -Z_0 \end{bmatrix} \cdot \begin{bmatrix} \tilde{i}_L \\ \tilde{u}_c \\ \tilde{i}_0 \end{bmatrix} + \begin{bmatrix} 1-D \\ 0 \\ D-1 \end{bmatrix} \cdot \tilde{u}_{IN} + \begin{bmatrix} 2U_C - U_{IN} \\ -2I_L + I_0 \\ -2U_C + U_{IN} \end{bmatrix} \cdot \tilde{d} \qquad (6)$$

Where $D=D_0$. Further, by applying the Laplace transformation to Eq. (6), we can write:

$$\begin{cases} s\cdot L\cdot \tilde{i}_L(s) = (2D-1)\cdot\tilde{u}_c(s) + (1-D)\cdot\tilde{u}_{IN}(s) + \\ \quad + (2U_C - U_{IN})\cdot\tilde{d}(s); \\ s\cdot C\cdot\tilde{u}_c(s) = (1-2D)\cdot\tilde{i}_L(s) + (D-1)\cdot\tilde{i}_0 + \\ \quad + (-2I_L + I_0)\cdot\tilde{d}(s); \\ s\cdot L_0\cdot\tilde{i}_0(s) = (2-2D)\cdot\tilde{u}_c(s) - Z_0(s)\cdot\tilde{i}_0 + \\ \quad + (D-1)\cdot\tilde{u}_{IN}(s) - (2U_C - U_{IN})\cdot\tilde{d}(s). \end{cases} \qquad (7)$$

On the basis of derived dependencies (7) it is easy to determine appropriate transfer functions for the output response. The small signal perturbations of the input voltage $\tilde{u}_{IN}(s)$ and of the shoot-through duty cycle $\tilde{d}(s)$ define the output voltage variations. Assuming a non-variable input voltage $\tilde{u}_{IN}(s)=0$, we will obtain a transfer function that describes the output voltage behavior for shoot-through duty cycle variations.

Taking into account the load Z_0 at the operating point (I_0, U_{IN}, U_C, D, I_L) and also assuming that

$$Z_0(s) = R_0/(C_0\cdot R_0\cdot s + 1), \qquad (8)$$

we can evaluate the dynamic behavior of the qZS-converter of the small signal transfer function as follows:

$$\tilde{u}_0(s)/\tilde{d}(s) = L_1(s)/M_1(s), \qquad (9)$$

where:

$$L_1(s) = R_0\cdot U_{IN} + \left[2\cdot R_0\cdot L\cdot(D-1)\cdot(2\cdot I_L - I_0)\right]\cdot s + \left[R_0\cdot L\cdot C\cdot(U_{IN} - 2\cdot U_C)\right]\cdot s^2, \qquad (10)$$

$$M_1(s) = \left\{L_0\cdot L\cdot C\cdot C_0\cdot R_0\right\}\cdot s^4 + \left\{L_0\cdot L\cdot C\right\}\cdot s^3 + \left\{\begin{matrix} +L\cdot R_0\cdot\left[2\cdot C_0\cdot\left(1+D^2-2\cdot D\right)+C\right] \\ +L_0\cdot C_0\cdot R_0\cdot\left(4D^2-4D+1\right) \end{matrix}\right\}\cdot s^2 + \left\{L_0\cdot\left(1-4\cdot D+D^2\right)+2\cdot L\cdot\left(1-2\cdot D+D^2\right)\right\}\cdot s + R_0\cdot\left\{1-4D+4D^2\right\} \qquad (11)$$

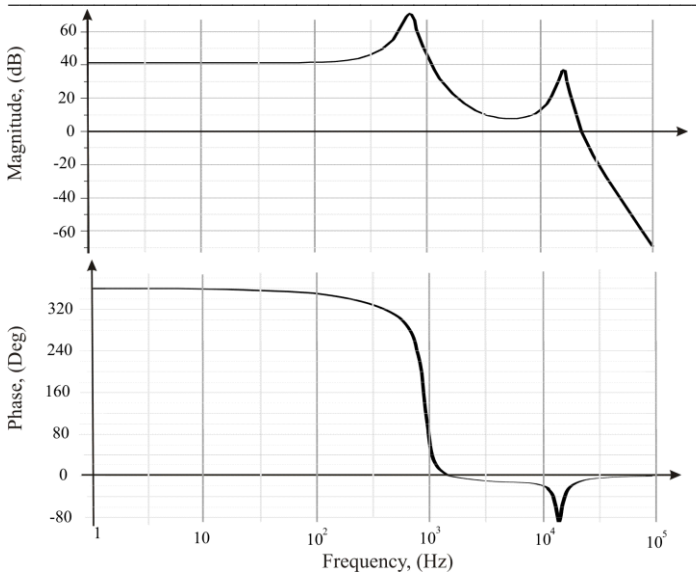

Fig. 3. Bode diagram of the qZS-converter.

Fig. 3 presents the Bode diagram drawn on the basis of Eq. (9). It was plotted for the operating parameters U_{IN} = 30 V, R_O = 5 Ω and component values L = 65 μH, C = 180 μF, L_O = 10 μH, C_O = 10 μF. The nominal value of the shoot-through duty cycle was set at D_0 = 0.25. Currents I_L, I_0 and voltage U_C were determined from the static model presented in [4].

The diagram for higher frequencies (about 1 kHz) shows that there is a need of careful selection of settings to assure stability of the arrangement and high control dynamics without oscillations and a need for significant readjustment.

III. CAEB QZS-CONVERTER

Fig. 4 illustrates the dynamic model of the CAEB qZS-converter, which regards the CCM, and in which the diodes D_1 and D_2 (Fig.1*b*) were replaced with switches $\overline{S}$. The full–bridge inverter is replaced by the switch *S*.

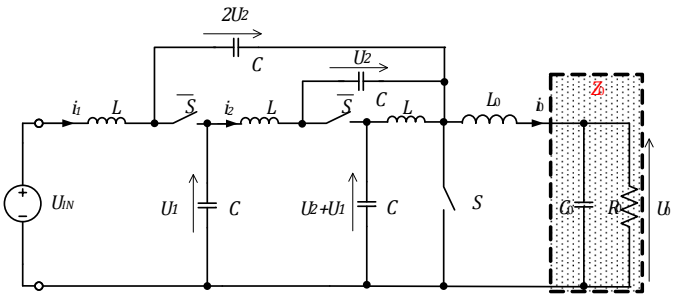

Fig. 4. Lossless dynamic model of the CAEB qZS-converter.

As in the previous case the ratios of currents and voltages were determined from the static model [12]. The state space model is described by the differential Eqs. (12) and (13) for the shoot-through state and active state, respectively.

In equations U=U_{IN} and D_0+D_1=1 are the same as in the previous situation (since the CCM is under consideration).

$$\begin{bmatrix} L\frac{di_1}{dt} \\ L\frac{di_2}{dt} \\ C\frac{du_1}{dt} \\ C\frac{du_2}{dt} \\ L_0\frac{di_0}{dt} \end{bmatrix} = \underbrace{\begin{bmatrix} 0 & 0 & 0 & 2 & 0 \\ 0 & 0 & 1 & 1 & 0 \\ 0 & -1 & 0 & 0 & 0 \\ 0 & -1 & 0 & 0 & 0 \\ 0 & 0 & 0 & 0 & -Z_0 \end{bmatrix}}_{A_1} \cdot \underbrace{\begin{bmatrix} i_1 \\ i_2 \\ u_1 \\ u_2 \\ i_0 \end{bmatrix}}_{X} + \underbrace{\begin{bmatrix} 1 \\ 0 \\ 0 \\ 0 \\ 0 \end{bmatrix}}_{B_1} \cdot U \quad (12)$$

$$\begin{bmatrix} L\frac{di_1}{dt} \\ L\frac{di_2}{dt} \\ C\frac{du_1}{dt} \\ C\frac{du_2}{dt} \\ L_0\frac{di_0}{dt} \end{bmatrix} = \underbrace{\begin{bmatrix} 0 & 0 & -1 & 0 & 0 \\ 0 & 0 & 0 & -1 & 0 \\ 1 & 0 & 0 & 0 & 0 \\ 0 & 1 & 0 & 0 & 0 \\ 0 & 0 & 1 & 2 & -Z_0 \end{bmatrix}}_{A_2} \cdot \underbrace{\begin{bmatrix} i_1 \\ i_2 \\ u_1 \\ u_2 \\ i_0 \end{bmatrix}}_{X} + \underbrace{\begin{bmatrix} 1 \\ 0 \\ 0 \\ 0 \\ 0 \end{bmatrix}}_{B_2} \cdot U \quad (13)$$

Taking into account equations describing the model of the converter and matrixes A_1, A_2, B_1, B_2 included in the matrix equations as well as the fact that in the case of CCM we have D_1=1-D_0, we obtain a small signal model:

$$\begin{bmatrix} L\frac{d\tilde{i}_1}{dt} \\ L\frac{d\tilde{i}_2}{dt} \\ C\frac{d\tilde{u}_1}{dt} \\ C\frac{d\tilde{u}_2}{dt} \\ L_0\frac{d\tilde{i}_0}{dt} \end{bmatrix} = \begin{bmatrix} 0 & 0 & -1+D & 2D & 0 \\ 0 & 0 & D_S & 2D-1 & 0 \\ 1-D & -D & 0 & 0 & 0 \\ 0 & -1 & 0 & 0 & 0 \\ 0 & 0 & 1-D & 2(1-D) & -Z_0(2D-1) \end{bmatrix} \times \quad (14)$$

$$\times \begin{bmatrix} \tilde{i}_1 \\ \tilde{i}_2 \\ \tilde{u}_1 \\ \tilde{u}_2 \\ \tilde{i}_0 \end{bmatrix} + \begin{bmatrix} 1 \\ 0 \\ 0 \\ 0 \\ 0 \end{bmatrix} \cdot \tilde{u}_{IN} + \begin{bmatrix} U_1 + 2U_2 \\ U_1 + 2U_2 \\ -I_1 - I_2 \\ I_1 \\ U_1 + 2U_2 - I_0 Z_0 \end{bmatrix} \cdot \tilde{d}$$

Further, by applying the Laplace transformation to Eq. (14), we can write:

$$\begin{cases} s \cdot L \cdot \tilde{i}_1(s) = (D-1) \cdot \tilde{u}_1(s) + 2D \cdot \tilde{u}_2(s) + \tilde{u}_{IN} + \\ + (U_1 + 2U_2) \cdot \tilde{d}(s), \\ s \cdot L \cdot \tilde{i}_2(s) = D \cdot \tilde{u}_1(s) + (2D-1) \cdot \tilde{u}_2(s) + \\ + (U_1 + 2U_2) \cdot \tilde{d}(s), \\ s \cdot C \cdot \tilde{u}_1(s) = (1-D) \cdot \tilde{i}_1(s) - D \cdot \tilde{i}_2(s) - \\ - (I_1 + I_2) \cdot \tilde{d}(s), \\ s \cdot C \cdot \tilde{u}_1(s) = -\tilde{i}_2(s) + I_1 \cdot \tilde{d}(s), \\ s \cdot L_0 \cdot \tilde{i}_0(s) = (1-D) \cdot \tilde{u}_1(s) + 2(1-D) \cdot \tilde{u}_2 - \\ - (2D-1) Z_0(s) \cdot \tilde{i}_0 + (U_1 + 2U_2 - I_0 Z_0) \cdot \tilde{d}. \end{cases} \quad (15)$$

$$L_2(s) = -R_0 \cdot \{(U_1 + 2U_2) \cdot (4 - 10D + 6D^2) - I_0 \cdot R_0 (1 + 3D^2 - 4D) + s \cdot (C_0 \cdot R_0 \cdot (U_1 + 2U_2) \cdot (4 - 10D + 6D^2) + L \cdot I_1 \cdot (4D - D^2 - 3) + L \cdot I_2 \cdot (D - 1)) +$$
$$+ s^2 \cdot (2L \cdot C \cdot D^2 \cdot I_0 \cdot R_0 + L \cdot C \cdot (U_1 + 2U_2)(D - 4D^2 + 2) + L \cdot C_0 \cdot R_0 \cdot (D - 1) \cdot (3I_1 + I_2)) + s^3 \cdot (L \cdot C \cdot C_0 \cdot R_0 \cdot (U_1 + 2U_2) \cdot (D - 4D^2 + 1) +$$
$$+ L^2 \cdot C \cdot (I_1 - I_2) \cdot (D - 1)) + s^4 (L^2 \cdot C^2 \cdot I_0 \cdot R_0 - L^2 \cdot C^2 \cdot (U_1 + 2U_2) + L^2 \cdot C \cdot C_0 \cdot R_0 \cdot (D - 1) \cdot (I_1 - I_2)) - s^5 \cdot L^2 \cdot C^2 \cdot (U_1 + 2U_2)\}. \quad (16)$$

$$M_2(s) = \{L_0 \cdot L^2 \cdot C^2 \cdot C_0^2 \cdot R_0^2\} \cdot s^7 + \{2L_0 \cdot C_0 \cdot R_0 \cdot L^2 \cdot C^2\} \cdot s^6 + \{L_0 \cdot L^2 \cdot C^2 + L^2 \cdot C^2 \cdot C_0 \cdot R_0^2 (2D - 1) + 2D^2 \cdot L \cdot C \cdot C_0^2 \cdot R_0^2\} \cdot s^5 +$$
$$+ \{4D^2 \cdot L_0 \cdot L \cdot C \cdot C_0 \cdot R_0 + L^2 \cdot C^2 \cdot R_0 (2D - 1)\} \cdot s^4 + \{L_0 \cdot C_0^2 \cdot R_0^2 \cdot (4D - 3D^2 - 1) + L \cdot C \cdot C_0 \cdot R_0^2 (4D^3 - 2D^2) + 2D^2 \cdot L \cdot C \cdot L_0\} \cdot s^3 +$$
$$+ \{L \cdot R_0 \cdot C \cdot (4D^3 - 2D^2) + L_0 \cdot C_0 \cdot R_0 \cdot (8D - 6D^2 - 2)\} \cdot s^2 + \{L_0 \cdot (4 \cdot D - 3D^2 - 1) + C_0 \cdot R_0^2 \cdot (1 - 6 \cdot D + 11D^2 - 6D^3)\} \cdot s + R_0 \cdot \{1 - 6D + 11D^2 - 6D^3\}. \quad (17)$$

Assuming $\tilde{u}_{IN}(s) = 0$, we can obtain the transfer function on the basis of derived dependencies (15). Load Z_0 is at the operating point $(I_0, U_{IN}, U_1, U_2, D, I_1, I_2)$.

We can evaluate the dynamics of changes in the output voltage of the CAEB qZS-converter with the changes in the shoot-through duty cycle D_0. The transfer function describing this dynamics is defined in the same way as (9) and represented by Eqs. (16) and (17).

Fig. 5 presents the Bode diagram based on the transfer function. It was determined for the same operating parameters and component values. The nominal value of the shoot-through duty cycle was set at $D_0 = 0.17$, voltages $U_1 = 40$ V and $U_2 = 10$ V.

As in the traditional qZS-converter, running of the diagram for higher frequencies is significant, as it indicates the necessity to assure stability of the arrangement and high control dynamics, without oscillations and a need for significant readjustment. The amount of reactive elements was increased. Such systems are more complicated because of the higher order of the transfer function.

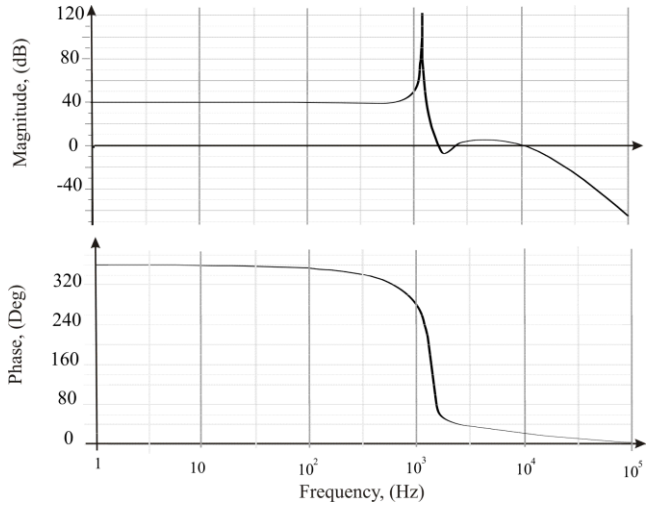

Fig. 5. Bode diagram of the CAEB qZS-converter.

IV. DAEB QZS-CONVERTER

Fig. 6 illustrates the lossless dynamic model of the DAEB qZS-converter. The diodes D_1 and D_2 (Fig. 1*c*) were replaced with switches $\bar{S}$, and the diode D_3 was replaced with the switch *S* synchronized with the main switch *S*.

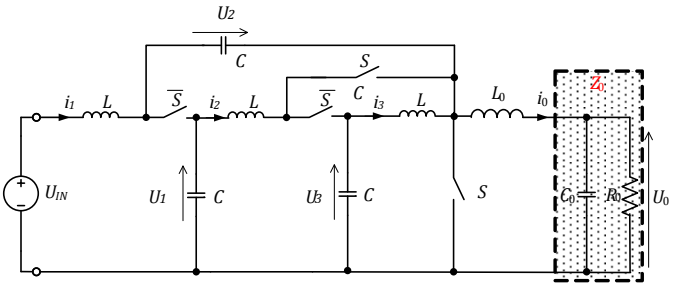

Fig. 6. Lossless dynamic model of the DAEB qZS-converter.

Compared to CAEB this scheme can be described by seven independent states:

- for the shoot-through mode (intervals of length $D_0 \cdot T$):

$$\begin{bmatrix} L\frac{di_1}{dt} \\ L\frac{di_2}{dt} \\ L\frac{di_3}{dt} \\ C\frac{du_1}{dt} \\ C\frac{du_2}{dt} \\ C\frac{du_3}{dt} \\ L_0\frac{di_0}{dt} \end{bmatrix} = \underbrace{\begin{bmatrix} 0 & 0 & 0 & 0 & 1 & 0 & 0 \\ 0 & 0 & 0 & 1 & 0 & 0 & 0 \\ 0 & 0 & 0 & 0 & 0 & 1 & 0 \\ 0 & -1 & 0 & 0 & 0 & 0 & 0 \\ -1 & 0 & 0 & 0 & 0 & 0 & 0 \\ 0 & 0 & -1 & 0 & 0 & 0 & 0 \\ 0 & 0 & 0 & 0 & 0 & 0 & -Z_0 \end{bmatrix}}_{A_1} \times \underbrace{\begin{bmatrix} i_1 \\ i_2 \\ i_3 \\ u_1 \\ u_2 \\ u_3 \\ i_0 \end{bmatrix}}_{X} + \underbrace{\begin{bmatrix} 1 \\ 0 \\ 0 \\ 0 \\ 0 \\ 0 \\ 0 \end{bmatrix}}_{B_1} \times U \quad (18)$$

- in the active mode (intervals of length $D_1 \cdot T$):

$$\begin{bmatrix} L\frac{di_1}{dt} \\ L\frac{di_2}{dt} \\ L\frac{di_3}{dt} \\ C\frac{du_1}{dt} \\ C\frac{du_2}{dt} \\ C\frac{du_3}{dt} \\ L_0\frac{di_0}{dt} \end{bmatrix} = \underbrace{\begin{bmatrix} 0 & 0 & 0 & -1 & 0 & 0 & 0 \\ 0 & 0 & 0 & 1 & 0 & -1 & 0 \\ 0 & 0 & 0 & -1 & -1 & 1 & 0 \\ 1 & -1 & 1 & 0 & 0 & 0 & 1 \\ 0 & 0 & 1 & 0 & 0 & 0 & -1 \\ 0 & 1 & -1 & 0 & 0 & 0 & 0 \\ 0 & 0 & 0 & 1 & 1 & 0 & -Z_0 \end{bmatrix}}_{A_2} \times$$

$$\times \underbrace{\begin{bmatrix} i_1 \\ i_2 \\ i_3 \\ u_1 \\ u_2 \\ u_3 \\ i_0 \end{bmatrix}}_{X} + \underbrace{\begin{bmatrix} 1 \\ 0 \\ 0 \\ 0 \\ 0 \\ 0 \\ 0 \end{bmatrix}}_{B_2} \cdot U \tag{19}$$

Taking into account that $U=U_{IN}$, $D_0+D_1=1$ and also matrixes A_1, A_2, B_1, B_2 included in the matrix equations as well as the fact that in the case of CCM we have $D_1=1-D_0$, $D_0 = D$ we obtain:

$$A = \begin{bmatrix} 0 & 0 & 0 & D-1 & D & 0 & 0 \\ 0 & 0 & 0 & 1 & 0 & D-1 & 0 \\ 0 & 0 & 0 & D-1 & D-1 & 1 & 0 \\ 1-D & -1 & 1-D & 0 & 0 & 0 & 1-D \\ -D & 0 & 1-D & 0 & 0 & 0 & D-1 \\ 0 & 1-D & -1 & 0 & 0 & 0 & 0 \\ 0 & 0 & 0 & 1-D & 1-D & 0 & -Z_0 \end{bmatrix}, \tag{20}$$

$$B = \begin{bmatrix} 1 \\ 0 \\ 0 \\ 0 \\ 0 \\ 0 \\ 0 \end{bmatrix}$$

Further, based on Eq. (5) by applying the Laplace transformation to Eq. (20), we can write a system of equations in the state space (21).

$$\begin{cases} s\cdot L\cdot \tilde{i}_1(s) = (D-1)\cdot \tilde{u}_1(s) + D\cdot \tilde{u}_2(s) + \\ \quad + \tilde{u}_{IN} + (U_1+U_2)\cdot \tilde{d}(s), \\ s\cdot L\cdot \tilde{i}_2(s) = \tilde{u}_1(s) + (D-1)\cdot \tilde{u}_3(s) + U_3\cdot \tilde{d}(s), \\ s\cdot L\cdot \tilde{i}_3(s) = (D-1)\cdot (\tilde{u}_1(s) + \tilde{U}_2(s)) + \\ \quad + \tilde{u}_3(s) + (U_1+U_2)\cdot \tilde{d}(s), \\ s\cdot C\cdot \tilde{u}_1(s) = (1-D)\cdot \tilde{i}_1(s) - \tilde{i}_2(s) + (1-D)\cdot \tilde{i}_3(s) + \\ + (1-D)\cdot \tilde{i}_0(s) + (-I_1 - I_3 - I_0)\cdot \tilde{d}(s), \\ s\cdot C\cdot \tilde{U}_2(s) = -D\cdot \tilde{i}_1(s) + (1-D)\cdot \tilde{i}_3(s) + \\ \quad + (D-1)\cdot \tilde{i}_0(s) + (-I_1 - I_3 + I_0)\cdot \tilde{d}(s), \\ s\cdot C\cdot \tilde{u}_3(s) = (1-D)\cdot \tilde{i}_2(s) - \tilde{i}_3(s) - I_2\cdot \tilde{d}(s), \\ s\cdot L_0\cdot \tilde{i}_0(s) = (1-D)\cdot (\tilde{u}_1(s) + \tilde{u}_2(s)) - \tilde{i}_0(s)\cdot Z_0 - \\ - (U_1+U_2)\cdot \tilde{d}(s). \end{cases} \tag{21}$$

Assuming a load Z_0 at the operating point (I_0, U_{IN}, U_1, U_2, D, I_1, I_2), the numerator and the denominator of the transfer function in this case are expressed by Eqs. (22) and (23).

Fig. 7 presents the Bode diagram for a DAEB qZS converter constructed on the basis of Eqs. (22) and (23).

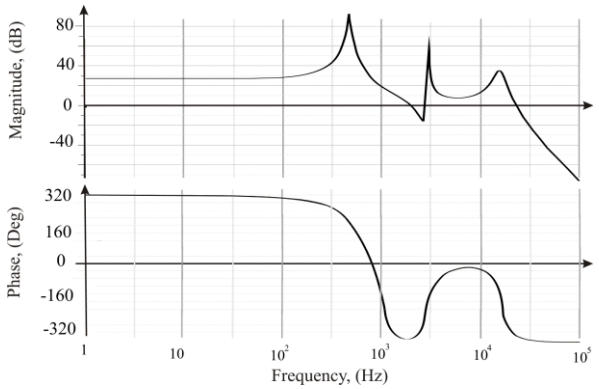

Fig. 7. Bode diagram of the DAEB qZS-converter.

The order of such systems is higher and their behavior is more complicated. As can we see from the figure, the DAEB qZS-converter leads to a phase shift at high frequencies that reverses on the poles. It can evoke instability in the system because of the higher order. It should be taken into account during the control system design.

$$\begin{aligned} L_3(s) = {} & R_0\cdot\{(U_1+U_2)\cdot(1-3D+D^2) - U_3(1+4D^2-4D) + s\cdot(L\cdot(I_1+I_3)\cdot(-3+5D-3D^2+D^3) + \\ & + L\cdot I_0\cdot(1-3D+5D^2-5D^3+2D^4) + L\cdot I_2\cdot(3D-5D^2-2)) + s^2\cdot(L\cdot C\cdot(U_1+U_2)(3D^2-5D-D^3) + \\ & + L\cdot C\cdot U_3\cdot(1-6D+7D^2-2D^3)) + s^3\cdot(L^2\cdot C\cdot(I_1+I_3)\cdot(10D+2D^3-6D^2) + \\ & + L^2\cdot C\cdot I_2\cdot(6D-3D^2) + L^2\cdot C\cdot I_2\cdot(2D^2-4D)) + s^4(L^2\cdot C^2\cdot(U_1+U_2)(D-D^2-3) + L^2\cdot C^2\cdot U_3(D-1)) + 2s^5\cdot L^3\cdot C^2\cdot(I_1+I_3)(D-1)\}. \end{aligned} \tag{22}$$

$$\begin{aligned} M_3(s) = {} & \{L_0\cdot L^3\cdot C^3\cdot C_0\cdot R_0\}\cdot s^8 + \{L_0\cdot L^3\cdot C^3\}\cdot s^7 + \{L^3\cdot C^3\cdot R_0 - L^2\cdot C^2\cdot L_0\cdot C_0\cdot R_0(8D-5D^2-6)\}\cdot s^6 + \{L_0\cdot L^2\cdot C^2\cdot(6+D^2-8D)\}\cdot s^5 + \{L_0\cdot L\cdot C\cdot \\ & \times C_0\cdot R_0\cdot(5-14D+22D^2-14D^3+4D^4) + L^2\cdot C^2\cdot R_0(6-8D+5D^2) + L^2\cdot C\cdot C_0\cdot R_0\cdot(2-6D+6D^2-2D^3)\}\cdot s^4 + \{L\cdot C\cdot L_0(1-14D+22D^2-14D^3+ \\ & + 4D^4) + \cdot L^2\cdot C\cdot(2-6D+6D^2-2D^3)\}\cdot s^3 + \{L\cdot R_0\cdot C\cdot(4D^4-14D^3) + L_0\cdot C_0\cdot R_0\cdot(6D++11D^2-6D^3+D^4) + L\cdot C_0\cdot R_0\cdot\left(8D^2-10D^3+7D^4-2D^5\right)\}\cdot s^2 + \\ & + \{L_0\cdot\left(1-6\cdot D+11D^2-6D^3+D^4\right) + L\cdot\left(1-4D+8D^2-10D^3+7D^4-2D^5\right)\}\cdot s + R_0\cdot\{1-6D+11D^2-6D^3+D^4\}. \end{aligned} \tag{23}$$

V. CONCLUSIONS

Lossless dynamic models of the qZS-converter family are presented in this paper. An AC small signal model allowed obtaining transfer function of the output voltage response from shoot-through duty cycle variations. It should be noted that it is inadmissible to use this model and the transfer function to obtain the transient process of response. Assumptions accepted during the analysis limit us. First, the wide range of shoot-through duty cycle variations during the transient process contradicts the AC small signal model. Also, the operating point of the transfer function in such models is chosen according to the average states in the converter and cannot be changed in a wide range.

On the other hand, the results obtained are relevant and should be taken into account during a close loop control system design.

To provide constant output voltage a close loop digital control system admits shoot-through duty cycle variations. In this case problems with stability can occur. Bode diagrams of the observed converters show that on the resonance frequencies of shoot-through duty cycle variations the gain factor significantly increases and the phase shift changes rapidly. It can evoke an unpredictable situation and loss of stability. Based on the analysis of the transfer functions obtained it is obvious that resonance frequencies are defined by the elements and the operating point of the converter and can be easily calculated. To avoid stability problems the speed of shoot-through duty cycle variations must be limited. It is especially relevant in digital control systems where the processes are discrete and connected with the system clock frequency.

Resulting from the topologies studied it is obvious that the CAEB qZS topology has better dynamics characteristics than the traditional qZS and DAEB qZS converters and could be recommended for applications where high input voltage gain and increased reliability are demanded.

ACKNOWLEDGMENT

This research work has been supported by Estonian Ministry of Education and Research (Project SF0140016s11) and Estonian Science Foundation (Grants ETF8538 and ETF8687).

REFERENCES

[1] Anderson, J.; Peng, F.Z., "Four quasi-Z-Source inverters", in Proc. of IEEE Power Electronics Specialists Conference, PESC'2008. pp. 2743-2749, 15-19 June 2008.

[2] Yuan Li; Anderson, J.; Peng, F.Z.; Dichen Liu, "Quasi-Z-Source Inverter for Photovoltaic Power Generation Systems", in Proc. of IEEE Applied Power Electronics Conference and Exposition APEC'2009, pp. 918-924, 15-19 Feb. 2009.

[3] Jong-Hyoung Park; Heung-Geun Kim; Eui-Cheol Nho; Tae-Won Chun; Jaeho Choi, "Grid-connected PV System Using a Quasi-Z-source Inverter", in Proc. of IEEE Applied Power Electronics Conference and Exposition APEC'2009, pp. 925-929, 15-19 Feb. 2009.

[4] Strzelecki, R., Vinnikov, D., "Models of the qZ-Converters". *Electrical Review*, vol. 86, no. 6, pp. 80-84, 2010.

[5] C. J. Gajanayake, F. L. Luo, H. B. Gooi, P. L. So, L. K. Siow, "Extended boost Z-source inverters", in Proc. *IEEE Conf. ECCE'09*, pp. 3845-385, Sept. 2009.

[6] Gajanayake, C.J.; Gooi, H.B.; Luo, F.L.; So, P.L.; Siow, L.K.; Vo, Q.N., "Simple modulation and control method for new extended boost quasi Z-source," in Proc. of 2009 IEEE Region 10 Conference *TENCON'2009*, pp. 1-6, 23-26 Jan. 2009.

[7] Strzelecki, R., Adamowicz, M., "Boost-buck inverters with cascaded qZ-type impedance networks", *Electrical Review*, vol. 86, no. 2, pp. 370-375, 2010.

[8] M. Adamowicz, R. Strzelecki, D. Vinnikov, "Cascaded Quasi-Z-Source Inverters for Renewable Energy Generation Systems", in Proc. *Ecologic Vehicles and Renewable Energies Conference EVER'10*, March 2010.

[9] D. Vinnikov, I. Roasto, R. Strzelecki, M. Adamowicz, "Performance Improvement Method for the Voltage-Fed qZSI with Continuous Input Current", in Proc. *IEEE Mediterranean Electrotechn. Conf. MELECON'10*, April 2010.

[10] Vinnikov, D.; Roasto, I.; Jalakas, T., "Comparative study of capacitor-assisted extended boost qZSIs operating in continuous conduction mode", in Proc. *12th Biennial Baltic Electronics Conference (BEC'2010),* pp. 297-300, 4-6 Oct. 2010.

[11] Vinnikov, D., Roasto, I.; Strzelecki, R., Adamowicz, M., "Two-Stage Quasi-Z-Source Network Based Step-Up DC/DC Converter", in Proc. of IEEE International Symposium on Industrial Electronics ISIE'2010, pp. 1143-1148, July 4-7, 2010.

[12] Vinnikov, D.; Roasto, I., "Impact of Component Losses on the Voltage Boost Properties and Efficiency of the qZS-Converter Family", in Proc. *7th International Conference-Workshop Compatibility and Power Electronics (CPE'2011)*, pp. 303-308, 1-3 June 2011.

Dmitri Vinnikov received the Dipl.Eng, M.Sc. and Dr.Sc.techn. degrees in electrical engineering from Tallinn University of Technology, Tallinn, Estonia, in 1999, 2001 and 2005, respectively.

He is presently a Senior Researcher in the Department of Electrical Drives and Power Electronics, Tallinn University of Technology. He has authored more than 100 published papers on power converters design and development and is the holder of several Utility Models in this application field. His research interests include switchmode power converters, modeling and simulation of power systems, applied design of power converters and control systems and application and development of energy storage systems.

Oleksandr Husev received the B.Sc. and M.Sc. degrees in industrial electronics from Chernihiv State Technological University, Chernihiv, Ukraine, in 2007 and 2008 respectively, where he is currently working toward the PhD degree. His PhD thesis is devoted to research active power filters and development of control system based on artificial intellect.

He is assistant of the Department of Industrial Electronics, Chernihiv State Technological University and currently cooperates with the Department of Electrical Drives and Power Electronics, Tallinn University of Technology. He has over 10 publications and is the holder of several Patents.

His research interests are in control systems for power electronic converters based on a wide range of algorithms, including modeling, design, and simulation.

Indrek Roasto received the B.Sc and M.Sc degrees in electrical engineering from Tallinn University of Technology, Tallinn, Estonia, in 2003 and 2005, respectively. At the end of 2009 he defended the PhD thesis devoted to the research and development of smart control and protection systems for the high voltage high power galvanically isolated DC/DC converters.

At the present time he is a researcher in the Department of Electrical Drives and Power Electronics. He has over 30 publications and owns two Utility Models in the field of power electronics.

His research interests are in digital control of switching power converters, including modelling, design, and simulation.